Advances in Engineering Research : Possibilities and Challenges
ISSN Print: 3079-5192
ISSN Online: 3079-5206
https://doi.org/10.63313/AERpc.9030

Active Terahertz Surface Plasmon Polariton Multi-focal Focusing Lens based on Graphene Metasurface

Yifan Tang. Huirong Wang. Quan Li and Tai Chen
School of Electronic Engineering, Tianjin University of Technology and Education, Tianjin 300222, China
Email: Eunecter@outlook.com

How to cite this paper: Tang, Y. F., Wang, H. R., Li, Q., & Chen, T. (2025). Active Terahertz Surface Plasmon Polariton Multi-focal Focusing Lens based on Graphene Metasurface. Advances in Engineering Research : Possibilities and Challenges, 1(3), 83–89. ISSN Print: 3079-5192; ISSN Online: 3079-5206.
https://doi.org/10.63313/AERpc.9030
Published: 2025-06-27

Abstract

Terahertz (THz) focusing lenses, as crucial components for manipulating THz wavefronts and achieving energy concentration, play a vital role in fields such as THz imaging, sensing, and communication. Therefore, in this work, we de-signed and simulated an active terahertz surface plasmon polariton (SPP) mul-ti-focal focusing lens based on graphene. The lens consists of four concentric slit resonator rings (SRRs). By integrating graphene onto each SRR and applying bias voltages, the device achieves independent "ON/OFF" control over the SPP excitation efficiency for any two selected slit resonator rings. This allows for dynamic switching at the same operating frequency to produce various distinct focal distributions. Our design not only offers a new avenue for realizing com-pact and multifunctional THz wavefront manipulation devices but also demon-strates significant potential for future applications in areas such as THz dynamic beam shaping and reconfigurable imaging.

Keywords

Terahertz; Surface plasmon polariton; Multi-focal focusing lens; Graphene

1. Introduction

Terahertz waves, typically defined within the frequency range of 0.1 to 10 THz and occupying a unique spectral band in the electromagnetic spectrum between microwave and infrared light, possessing distinct physical properties such as strong penetration, low photon energy, and molecular fingerprinting characteristics, consequently demonstrate significant application potential in numerous cutting-edge fields including communication [1-3], sensing [4-6], and imaging [7-9]. Surface Plasmon Polaritons (SPPs) are a special type of electromagnetic wave, a mode formed by the coupling of light with free electrons on a metal surface. They are confined to propagate along the metal-dielectric interface, decaying exponentially in both directions perpendicular to the interface, and are capable of achieve localized field enhancement and propagation control at subwavelength scales. These unique physical properties have enabled SPPs to show great application potential in many frontier scientific and technological fields, such as holography [10,11], orbital angular momentum manipulation [12,13], and integrated plasmonic circuits [14].

Although SPPs exhibit numerous advantages, conventional SPP devices still face several challenges in practical applications. For instance, SPPs inevitably suffer from certain ohmic losses during propagation; concurrently, their coupling efficiency with free-space light is relatively low, and many existing SPP devices have relatively singular functionalities, making it difficult to meet the demands for multi-dimensional and fine-grained control of light fields in complex application scenarios. To effectively overcome these shortcomings and achieve precise manipulation of SPP wavefronts, the design of efficient SPP functional devices, especially lens structures capable of converging and guiding SPP energy, has become a key research focus.

To address these challenges, this paper proposes a multi-focal focusing lens based on slit resonator rings operating in the terahertz band. The proposed lens comprises four concentric slit resonator rings. By selectively activating any two of these rings, the lens is can generate distinct focal patterns with varying numbers of focal spots at its focal plane. We investigated and analyzed the multi-focal control capabilities of the designed lens using numerical simulations. Simulation results indicate that the designed lens can effectively produce well-defined multiple foci and demonstrates excellent focusing performance. This work holds significant potential for applications in multi-point sensing and integrated photonics.

2. Design Strategy

The proposed metasurface design is based on slit resonators (SRs), widely used in metasurface design for their effective coupling of free-space light to SPPs. For a single SR resonator, SPPs are excited only with polarization perpendicular to the slit, the SPPs excited by the parallel polarization component being much weaker, allowing it to be regarded as a dipole source perpendicular to the slit [15]. For circular polarization $E_{in} = (\sqrt{2}/2) \times (1, i\sigma)$ normally incident from the backside with σ standing for the spin direction of left-handed circular polarization (LCP) and right-handed circular polarization (RCP), according to the two-dimensional Huygens' principle, the SPP electric field at an arbitrary point *P* can be expressed as [11]:

$$E_P = \eta \frac{\sqrt{2}}{2} \frac{\exp(ik_{SP}|\boldsymbol{r}|)}{i\sqrt{\lambda_{SP}|\boldsymbol{r}|}} (\cos\theta + i\sigma \sin\theta) \cos(\theta - \xi) \tag{1}$$

where η is the complex coefficient describing the conversion efficiency of SPP excitation from the incident light E_{in} and the phase shift obtained from the dipole resonance; λ_{SP} and $k_{SP} = 2\pi / \lambda_{SP}$ are the wavelength and wavevector of the SPP; $\boldsymbol{r}$ is the vector from the dipole position to point *P*; ξ is the azimuth angle of point *P*, i.e., the angle between r and the x-axis; $\exp(ik_{SP}|\boldsymbol{r}|)$ and $1/\sqrt{|\boldsymbol{r}|}$ are the phase evolution and amplitude decay, respectively, according to the two-dimensional propagation characteristics of SPPs; the term $(\sqrt{2}/2)(\cos\theta + i\sigma\sin\theta)$ is the projection component in the direction perpendicular to the slit, and $\cos(\theta-\xi)$ is the inclination factor. By meticulously designing the orientation angle of each slit, and combining spin-dependent geometric phase with spin-independent propagation phase, the phase of the SPP excited by each SR and arriving at the target point can be independently controlled, thereby achieving arbitrary SPP wavefront manipulation. When the positions and orientation angles of all SRs are determined, assuming the device consists of n SRs, the superimposed SPPs at an arbitrary point *P* under circularly polarized incident light $E_{in} = (\sqrt{2}/2)\times(1, i\sigma)$ can be calculated as:

$$E_P = \eta\frac{\sqrt{2}}{2}\sum_n \frac{(\cos\theta_n + i\sigma\sin\theta_n)}{i\sqrt{\lambda_{SP}|\boldsymbol{L}_{np}|}}\exp(ik_{SP}|\boldsymbol{L}_{np}|)\cos\left[\theta_n - \arg(\boldsymbol{L}_{np})\right] \quad (2)$$

where θ_n is the orientation angle of *n*th SR; L_{np} is the vector from the center point of *n*th SR to the point *P*.

As discussed above, we propose a metasurface structure comprising four concentric rings of slit resonators. A schematic illustration of the proposed structure is presented in Figure 1(a). The device is composed of an aluminum (Al) pattern fabricated on a silicon (Si) substrate. Each of the four rings consists of 60 slit resonators. These concentric rings are located at radii of 1800 μm, 1900 μm, 2000 μm, and 2100 μm, respectively. The unit cell of these resonators is depicted in Figure 1(b), featuring geometric parameters of a = 70 μm and b = 10 μm. The specific position and orientation angle of each slit resonator are meticulously designed to achieve the desired focusing effect. The silicon substrate has a thickness of 650 μm, while the aluminum film is 0.2 μm thick.

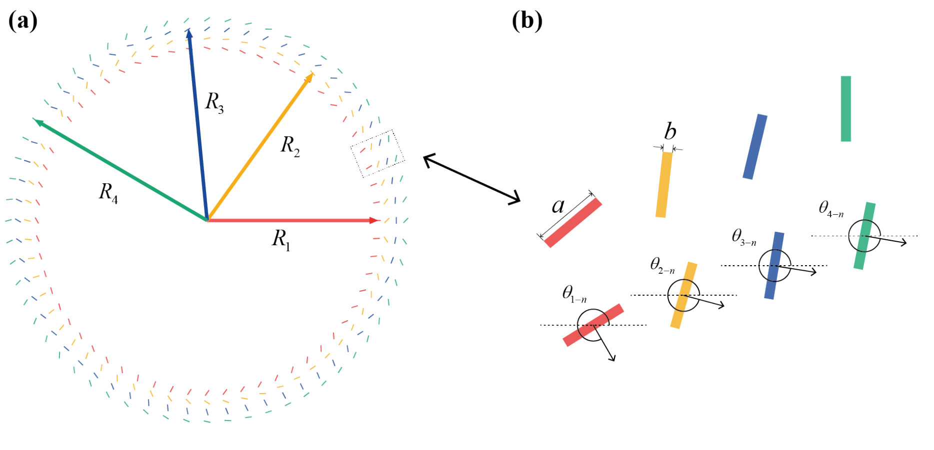

Figure 1. Schematic diagram of the multi-focal focusing lens. (a) Schematic of the overall structure; (b) Schematic of the unit cell.

When any two SRRs are active, the device can generate focal distributions with varying numbers and positions of foci. To achieve active control, graphene, a material with tunable conductivity, is integrated onto the surface of the SRs. Its conductivity characteristics can be collectively described by the intraband (σ_{intra}) and interband (σ_{inter}) transitions of the Kubo model [16]:

$$\sigma_g = \sigma_{\text{intra}} + \sigma_{\text{inter}} = i\frac{e^2 k_B T}{\pi \hbar^2(\omega + i\tau^{-1})}\left\{\frac{E_F}{k_B T} + 2\ln\left[\exp\left(-\frac{E_F}{k_B T}\right)+1\right]\right\} + i\frac{e^2}{4\pi\hbar}\ln\left[\frac{2|E_F| - \hbar(\omega + i\tau^{-1})}{2|E_F| + \hbar(\omega + i\tau^{-1})}\right] \quad (3)$$

where σ_g is the total conductivity of graphene; *e* is the elementary charge of an electron; k_B is Boltzmann's constant; $\hbar$ is the reduced Planck constant; *T* is a fixed temperature of 293 K; τ is the carrier relaxation time, which remains essentially constant under weak incident THz fields. E_F is the Fermi energy. Since the photon energy in the terahertz range is much smaller than the Fermi energy, the contribution of interband transitions can be neglected. Therefore, the surface conductivity σ_g is strongly dependent on its Fermi level E_F. When E_F increases from 0 eV to 0.8 eV, the conductivity of graphene significantly increases, causing it to transition from behaving like a dielectric to behaving like a metal. We define the Fermi level of 0 eV as the "ON" state and 0.8 eV as the "OFF" state. In the "ON" state, graphene has minimal impact on the SRRs, allowing the SRRs to effectively convert incident THz waves into SPPs. Conversely, in the "OFF" state, the highly conductive graphene shorts the covered SRRs, leading to a substantial reduction in SPP excitation efficiency and a significant weakening of the near-field intensity. This clearly demonstrates that by tuning the Fermi energy of graphene, the SRRs can be effectively switched between an "active" and "inactive" state.

3. Result and Discussion

Based on the graphene tuning mechanism, we conducted detailed simulation studies on the meticulously designed multi-focal lens. By setting the graphene on different rings to either the "ON" or "OFF" state, various dual-ring activation combinations were achieved. Simulations were performed using the commercial software CST Microwave Studio. The sample was modeled using aluminum and silicon from the CST material library. A plane wave is employed as the excitation source, vertically incident from the substrate side. The time-domain solver was used to compute a 5 mm × 5 mm area, with open boundary conditions applied in all directions. Electric field monitors were utilized to obtain the SPP electric field distribution maps, and the results are presented in Figure 2.

Under LCP light incidence, when the graphene on the inner ring R1 and the outer ring R3 was set to the "ON" state, while the graphene on rings R2 and R4 was in the "OFF" state, the simulated electric field intensity distribution in the focal plane is shown in Figure 2(a). The results reveal the formation of a clear four-foci pattern, with the foci arranged in an approximately symmetrical distribution. Subsequently, we switched the activation states, setting rings R2 and R4 to "ON" and rings R1 and R3 to "OFF". As depicted in Figure 2(b), a relatively diffuse single focus was observed in this configuration. The position and number of foci were significantly different from the previous mode, accompanied by some lower-intensity sidelobe structures. Compared to the distinct four-foci pattern in Figure 2(a), the focal separation and clarity were reduced in this mode; however, it still demonstrated the capability to converge incident energy to specific off-axis regions. Furthermore, two additional symmetric activation states were investigated: one where rings R1 and R4 were "ON" while R2 and R3 were "OFF", and another where rings R2 and R3 were "ON" while R1 and R4 were "OFF"., as shown in Figure 2(c) and (d), In both these configurations, a ring-shaped focus with a central dark area and energy concentrated in an annular region was formed. This was surrounded by concentric diffraction rings of gradually decreasing intensity, exhibiting good circular symmetry.

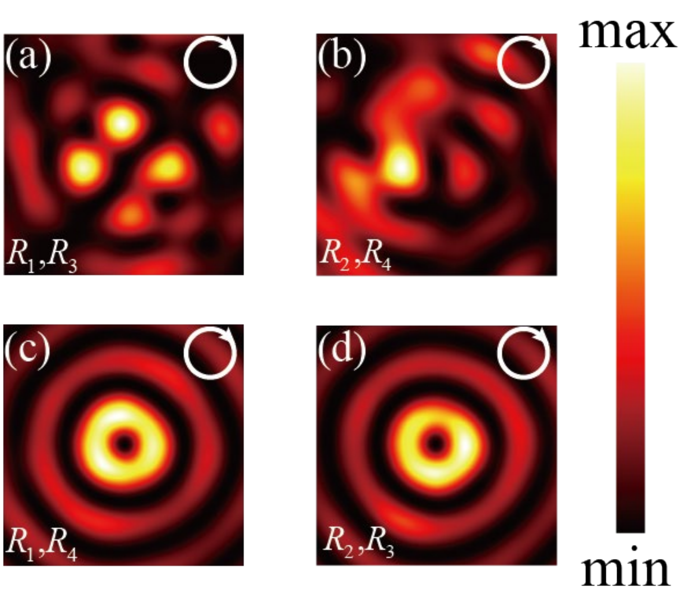

Figure 2. Simulated interference electric field distributions at 0.75 THz under LCP light incidence for different active ring pair configurations: (a) R1 & R3; (b) R2 & R4; (c) R1 & R4; (d) R2 & R3

Our design manipulates the light field by incorporating geometric phase control. For LCP and RCP light, the geometric phase introduces additional phase shifts that are equal in magnitude but opposite in sign. Although the phase details are conjugate, the physical mechanism and design objectives for modulating both polarizations by the structure are identical, leading to similar macroscopic physical effects, as illustrated in Figure 3. These simulation results clearly demonstrate that by selectively activating different pairs of resonator rings using graphene, the designed lens can achieve dynamically reconfigurable multi-focal focusing functionality in the terahertz band.

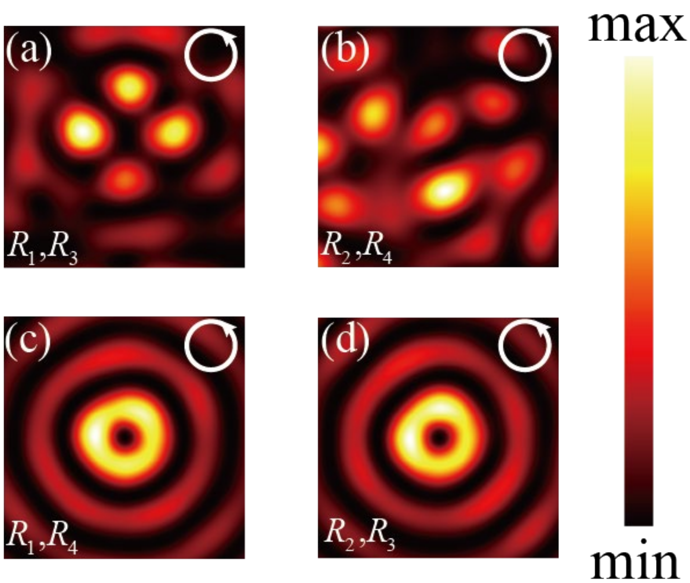

Figure 3. Simulated interference electric field distributions at 0.75 THz under RCP light incidence for different active ring pair configurations: (a) R1 & R3; (b) R2 & R4; (c) R1 & R4; (d) R2 & R3.

4. Conclusion

This paper presents the design and simulation of an active Terahertz multi-focal focusing lens based on slit resonator rings and graphene. We utilize the characteristic of graphene's conductivity varying with its Fermi energy to achieve independent and selective control over the operational state of each of the four SRRs, enabling the activation of desired dual-ring combinations. The multi-focal focusing characteristics of the designed structure at 0.75 THz were systematically investigated through simulations using the commercial software CST Microwave Studio. The simulation results clearly demonstrate that by selectively activating different dual-ring combinations, the lens can flexibly switch between multiple focusing modes on a single structure. This work not only provides new design concepts and feasible technical routes for developing compact, efficient, and functionally reconfigurable THz wavefront manipulation devices but also offers insights for achieving more complex light field manipulation.

Acknowledgements

This work was funded by the Scientific Research Plan Project of Tianjin Municipal Education Commission (2022KJ119).

References

[1] Xu, Z.H., He, J., Hao, X., et al. (2025) Quantitative terahertz communication evaluation of compact valley topological photonic crystal waveguides. *ACS Photonics*, **12**(4),

1822-1828.

[2] Chen, H., Ren, H., Wang, W., et al. (2024) Terahertz chiral edge states enable inner-chip state transition and interchip communications over wireless terminals. *Chinese Optics Letters*, **22**(10), 103701.

[3] Yang, Y., Yamagami, Y., Yu, X., et al. (2020) Terahertz topological photonics for on-chip communication. *Nature Photonics*, **14**, 446-451.

[4] Wang, Q., Chen, Y., Mao, J., et al. (2023) Metasurface-assisted terahertz sensing. *Sensors*, **23**, 5902.

[5] Wang, H., Zheng, F., Xu, Y., et al. (2023) Recent progress in terahertz biosensors based on artificial electromagnetic subwavelength structure. *Trends in Analytical Chemistry*, **158**, 116888.

[6] Xu, Y., Chen, X., Zhang, S., et al. (2024) Terahertz biochemical sensor based on multiparameter metasurface for molecular fingerprint detection. *Optics & Laser Technology*, **177**, 110959.

[7] Chen, J., Ding, K., Pi, Y., et al. (2024) Discriminative non-destructive imaging of flip chips based on photoacoustic remote sensing microscopy with layered elasto-optic models. *Optics Express*, **32**(13), 22700-22713.

[8] Chen, J., Ding, K., Pi, Y., et al. (2024) In-line imaging and recognition of flip chip fabrication defects by real-time photoacoustic remote sensing system. *Photoacoustics*, **38**, 100614.

[9] Wang, X., Wang, X., Yao, Z., et al. (2023) Digital imaging through terahertz mul-tifrequency programmable metasurface based on BIC. Optical Materials, 143, 114154.

[10] Liu, X., Wang, Q., Zhang, X., et al. (2019) Thermally dependent dynamic meta-holography using a vanadium dioxide integrated metasurface. *Advanced Optical Materials*, **7**, 1900175.

[11] Xu, Q., Zhang, X., Xu, Y., et al. (2017) Polarization-controlled surface plasmon holography. *Laser & Photonics Reviews*, **11**(1), 1600212.

[12] Jin, X., Wang, Z., Liu, M., et al. (2025) Vectorial beams with longitudinally varying polarizations generated by surface-wave metasurfaces. *Laser & Photonics Reviews*, **19**(2), 2402298.

[13] Zang, X., Zhu, Y., Mao, C., et al. (2018) Manipulating terahertz plasmonic vortex based on geometric and dynamic phase. *Advanced Optical Materials*, **6**(24), 1801328.

[14] Karnetzky, C., Zimmermann, P., Trummer, C., et al. (2018) Towards femtosecond on-chip electronics based on plasmonic hot electron nano-emitters. *Nature Communications*, **9**, 2471.

[15] Tanemura, T., Balram, K.C., Ly-Gagnon, D.S., et al. (2011) Multiple-wavelength focusing of surface plasmons with a nonperiodic nanoslit coupler. *Nano Letters*, **11**, 2693-2698.

[16] Chen, P.Y. and Alù, A. (2011) Atomically thin surface cloak using graphene monolayers. *ACS Nano*, **5**(7), 5855-5863.